

Ultraviolet Observations and a Theory of STEVE

Charles Lougheed Bennett^{1,1,1,1,1,1}

¹Lawrence Livermore National Laboratory

November 29, 2022

Abstract

A search was made for ultraviolet (UV) STEVE (Strong Thermal Emission Velocity Enhancement) in the DMSP database. In one 168 UV spectral channel case, low altitude UV continuum emission and high altitude 1304 Å + 1356 Å line emission were found. In 10 further cases, a two layer structure was found: 1356 Å emission at high altitude, and 1450±50 Å plus 1725±75 Å emission at low altitude. A theory is presented in which low altitude $e^* + O_2 \rightarrow O^- + O$ reactions produce O^- ions that subsequently drift upwards, followed by $O^+ + O^- \rightarrow O^* + O^*$ neutralization reactions yielding 1304 Å, 1356 Å and 6300 Å emissions. This theory explains the relative intensity of the observed 1304 Å and 1356 Å lines and predicts the intensity of the 6300 Å line relative to the ultraviolet lines.

Ultraviolet Observations and a Theory of STEVE

Charles L. Bennett¹

¹Retired from Lawrence Livermore National Laboratory, Livermore, CA, USA

Corresponding author: Charles Bennett (Charlie_Bennett@comcast.net)

Key Points:

- STEVE is found to only sometimes be associated with opposite hemisphere subauroral UV arcs in satellite data
- A database of 108 subauroral UV arcs and STEVE events found in data from 2005 to 2020 has been created
- An interplanetary magnetic field guided MeV solar proton precipitation theory quantitatively explains the systematics in this database.

Abstract

A search for ultraviolet (UV) emissions in satellite data during known STEVE (Strong Thermal Emission Velocity Enhancement) events found that simultaneous subauroral UV arcs (SUA) were not always present in the Southern Hemisphere despite coverage of the conjugate STEVE location. Over the years 2005 to 2020 a total of 108 SUA and STEVE cases were found. A theory is presented in which MeV solar protons guided by the interplanetary magnetic field (IMF) produce these arcs along with STEVE as they precipitate into the atmosphere. Numerous aspects of STEVE and SUA are explained by this theory.

Plain Language Summary

The mysterious glowing streaks of light known as "STEVE" seen together with the Northern Lights are currently not well understood. Scientists have long known that the Northern Lights are caused by electrons and protons precipitating into the earth's atmosphere and producing shimmering sheets of many colors. STEVE instead appears as a horizon to horizon narrow streak of purple light in the sky that cannot be explained by the usual electron and proton precipitation. In this work a novel theory is described in which very high energy protons from the sun bombard the atmosphere causing the air temperature to become extremely hot. So hot that the air becomes ionized, turning into a plasma fountain that may sometimes extend from the north pole to the south pole to create the light of STEVE in both hemispheres.

1 Introduction

STEVE appears from the ground as a narrow band of predominantly east-west oriented purple or whitish light, located equatorward of concurrent auroral activity (MacDonald, 2018) and sporadically accompanied by ephemeral green streaks termed the "picket fence". The picket fence features are found (Archer W. S.-L., 2019) to be at lower altitude than the purple/whitish features and aligned with the local magnetic field. STEVE has been found to be associated with unusually intense subauroral ion drift (SAID) events (Archer W. G.-L.-M., 2019). Visible light spectroscopy shows that the purple color is from $O(^1D)$ 6300 Å transitions with a broad continuum (Gillies D. D.-L., 2019). The picket fence has been found by (Mende S. a., 2019) to be predominantly $O(^1S)$ 5577 Å light with other spectral features that (Mende S. H., 2019) suggest argue against the assumption of perfect interhemispheric conjugacy and precipitating electrons as being the cause of the green features. In contrast (Nishimura Y. G.-L., 2019) argue in favor of electron precipitation and in favor of interhemispheric symmetry. This debate about the nature of STEVE has been underway since first raised by (Gallardo-Lacourt B. L., 2018).

In this work 35 STEVE events from (Gallardo-Lacourt B. N., 2018), (Mende S. a., 2019), (Gillies D. D.-L., 2019), (Chu, 2019), (Nishimura Y. G.-L., 2019), (Liang, 2019), (Archer W. G.-L.-M., 2019) and (Gillies D. L., 2020) were examined for the presence of ultraviolet (UV) emissions in Defense Meteorological Satellite Program (DMSP) data. Five of these events had no Subauroral Ultraviolet Arcs (SUA) in the Special Sensor Ultraviolet Spectrographic Imager (SSUSI) images in the Southern Hemisphere despite simultaneous conjugate coverage by at least one DMSP swath, indicating hemispheric asymmetry. The lack of hemispheric symmetry for the 5 April 2010 event was attributed by (Nishimura Y. Y., 2020) to its narrow latitudinal extent, but this seems implausible as several narrow SUA associated with dimmer STEVE are seen. A systematic search from 1 Jan 2005 through 31 Dec 2020 found 108 events that are published in

the (Bennett C. L., 2021) database. These observations led to the theory presented here of IMF guided MeV Proton Precipitation (IMF guided MPP).

2 Theory

Stopping power theory (Bethe, 1930) is used to analyze solar MPP. In Figure 1, an illustrative case for 1 to 10 MeV protons is considered. In **a** an exemplary pair of protons with guiding centers following the local IMF are schematically indicated. Whatever the pitch angles near the sun, in the smaller heliospheric magnetic field just outside the earth's magnetosphere (~ 6 nT), energetic protons have large gyroradii ($\sim 10 R_{\text{earth}}$) and small pitch angles. Northern and southern proton fluxes need not be equal. Higher (lower) energy protons penetrate to lower (higher) final altitudes before stopping (Berger, 2017), as shown in **1b**. The net total ionization rate (TIR) produced by a one MeV proton as a function of altitude computed with the GLOW model (Solomon, 2017) is shown in **1c**. The net TIR shown is the difference between $2 \text{ erg/cm}^2/\text{s}$ and $1 \text{ erg/cm}^2/\text{s}$ of proton flux that excludes non-protonic ionization. The values plotted in this figure are for the date, time and geographic location indicated in the plot, but the qualitative behavior is independent of the specific choices. It can be seen that the TIR has a narrow peak just below 100 km and vanishes at the stopping altitude. Higher or lower energy protons would have similar curves with the peak correspondingly displaced in altitude. The column integrated TIR per unit primary particle energy flux varies relatively slowly as a function of primary energy, as shown in **1e**. This slow variation with energy reflects the “rule of thumb” that the ionization produced by stopping high energy particles costs roughly 30 eV per ion pair. The overwhelming majority of secondary electrons produced in collisions along the stopping path are at low energy and leave the collision nearly perpendicular to the direction of the primary particle, as shown in **1d**, **1f**, and **1g**. The secondary electron distribution shown in **1h** follows (Edgar, 1973) and has a shape relatively insensitive to the primary energy. Because air atoms or molecules ionized in the stopping collisions typically gain but a few meV of energy, these ions retain the thermal kinetic energy distribution they had prior to ionization.

The cross sections for momentum transfer collisions between low energy electrons and N_2 molecules (Itikawa Y. , 2006) or O_2 molecules (Itikawa Y. , 2009) are approximately 10^{-15} cm^2 . Thus, given the variation of the column depth of the atmospheric constituents shown in **1i**, it is unlikely for most of the secondary electrons produced by high energy particles to emerge from below ~ 100 km without experiencing multiple inelastic collisions and heating the ambient atmosphere. Initially after the start of a period of MPP, with relatively cool ambient atmospheric temperature, most secondary electrons equilibrate to the ambient temperature, recombine with positive ions and do not escape the lower atmosphere. At this stage, beyond the heating of the atmosphere below 100 km, detectable by thermal emission continua in UV or visible light, there are few other detectable signatures of MPP. As MPP continues, the temperature of the atmosphere at the end of the range of the stopping particles may become sufficiently high that some of the hottest electrons and ions may avoid recombination. In the database, the average temperature from 32 Swarm crossings of SUA was 4.2 eV with the highest value being nearly 40 eV. These temperatures are high enough to produce significant thermal ionization. Newly ionized particles in this process spiraling around local magnetic field lines have a magnetic moment and are thus subject to an effective repulsion by the earth's magnetic field (Jursa, 1985) resulting in an upwelling flow of plasma. The upwelling plasma flow has a cooling effect that offsets the heating of MPP bombardment.

Under steady conditions, eventually the magnitude of the upwelling plasma flux would depend on the energy and intensity of the MPP as shown in **1e**. Under the typical sporadic conditions seen in the database (Bennett C. L., 2021) the upwelling flux relative to MPP is significantly less than shown in **1e**. In any case, the hot charged particles emerging from lower altitudes are not confined to the magnetic field lines of the primary particles due to multiple scattering. Thus even strongly localized MPP produces spatially broader regions of upwelling plasma. In the database 78 SUA had significant plasma flow that was without exception directed upwards with a mean of $2.3 \times 10^9 \text{ cm}^{-2}\text{s}^{-1}$. In cases where both thermal emission and upwelling plasma were seen, as in the second example shown below, the width of the plasma flow was substantially greater than the width of the thermal emission.

Because electrons are so much lighter than ions, with similar temperatures in the plasma, the upward flux of negative charge will be much greater than the upward flux of positive charge producing a net downward current flow. In the database 85 SUA exhibited downward Field Aligned Current (FAC).

Only an insignificant fraction of the TIR fraction shown in **1c** lies above the DMSP altitude ($\sim 850 \text{ km}$). As a result, few electrons would be seen in the DMSP SSJ detectors at the onset of MPP. However, once the “escape” threshold plasma temperature is reached, and as the “bounce” period for 30 eV electrons (the lowest SSJ channel) being magnetically reflected at the poles is approximately one minute, the spectrum of low energy electrons seen in the SSJ is expected to be strongly peaked at low energy, as shown in **1h** and would be seen almost simultaneously in both hemispheres leading to an upward FAC. In the database 46 SUA had intense localized Sub Auroral Low Energy Spikes (SALES) in the intensity of the lowest electron energy channel and 46 SUA had upward FAC. The up and down FACs had comparable flux. Both upwelling or downwelling electrons, in recombination reactions with O^+ in the ionosphere produce 1356 \AA emission. In 75 SUA, 1356 \AA emission dominated the UV color. The abundance of low energy electrons is also consistent with the (Mende S. H., 2019) observations.

Electrons moving at the same speed as solar MeV protons have only keV energy, and correspondingly lower magnetic rigidity. The earth’s magnetosphere ordinarily filters out these comoving electrons. For especially energetic MPP events, or for particularly weak magnetospheric filtering, a population of multi-keV electrons could co-precipitate with multi-MeV protons. Perhaps these circumstances are responsible for the appearance of the green picket fence feature of STEVE? If so, this would explain the finding (Bennett C. a., 2020) that the picket fence features share magnetic field lines with higher altitude purple STEVE features. Fluctuations in magnetospheric filtration could explain the ephemeral picket fence.

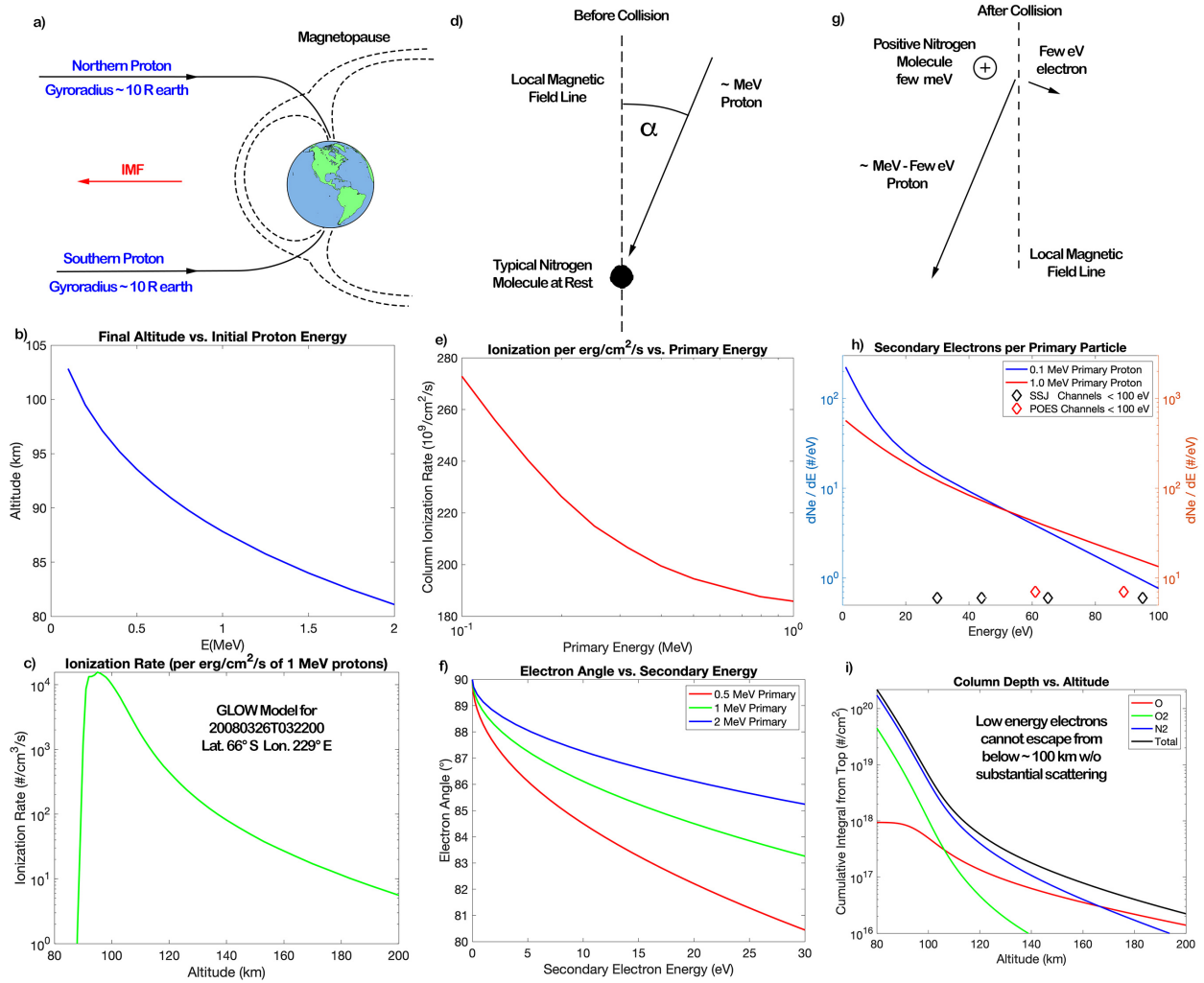


Figure 1. This figure illustrates the theory of IMF guided MeV Particle Precipitation into the earth's atmosphere.

3 Overview and Systematics of Database

The (Bennett C. L., 2021) database comprises a master spreadsheet and an overview figure for each event. This figure shows the SSUSI scans for both the Northern and Southern Hemispheres (NH and SH) for a single orbit in pseudocolor (red=1356 Å, green = LBH_{short}, blue = LBH_{long}) and orthographic projection assuming an altitude of 150 km with the DMSP ground track shown in white. SUA appear as red arcs just outside the equatorward auroral boundary (Ding, 2016) shown by the cyan curves. For the five cases of STEVE without SUA, the STEVE location and its magnetic conjugate are marked by open red pentagrams. Magenta pentagrams mark the position along the satellite orbit at SUA crossing times while matching cyan pentagrams mark the location projected along magnetic field lines to the altitude of the SSUSI scan. The IMF direction at one minute intervals is shown by orange circles. Polar Orbiting Environmental Satellites (POES) ground tracks over the duration of the DMSP orbit are shown in red with red pentagrams indicating the flux of protons above 6 MeV in the 0° telescope data, Swarm satellite ground tracks when available are shown in green with measurements of electron

temperature indicated by green pentagrams. The F16 DMSP satellite full spectral mode aim points when available are in blue.

The South Atlantic Anomaly (SAA) appears in POES data between 0° and 45° S latitude and between 10° and 90° W longitude because in the equatorial region 0° telescopes become sensitive to trapped particles, while in the auroral region they are only sensitive to precipitating particles. The fact that the Swarm temperature measurements seldom show spikes in the SAA while they often show spikes where POES data indicates MeV precipitation bolsters the veracity of the high Swarm temperatures (4.2 eV mean) seen while crossing SUA.

Contextual plots extending ± 6 hours from the start of the DMSP orbit show the MeV proton flux from Geostationary Operational Environmental Satellites (GOES), the IMF longitude and z-component. For 70 cases, this MeV flux significantly increases during SUA or STEVE events, despite separation by several earth radii, suggesting that simultaneous NH and SH MeV proton strikes are frequent but not universal.

The SUA DMSP crossings, excluding one outlier, were at 21.06 ± 0.89 MLT. The mean value and narrowness of this distribution are consistent with high rigidity (multi-MeV) protons following a Parker IMF spiral (Parker, 1963) but not following every transient fluctuation in IMF direction. Crossings near 9.0 MLT also consistent with the Parker spiral are sunlit and neither STEVE nor SUA could be seen.

Other features predicted by theory and verified in the database include:

1. upward plasma flow, 1356 Å emission and both upward and downward FACs latitudinally broader than a high temperature region;
2. frequent SALES of electrons but almost never ions;
3. 1356 Å emission at higher altitude than nominally “LBH” emission, here identified as continuum UV thermal emission indicative of high temperature
4. MPP spikes seen in POES crossings of SUA having widths matching SUA.

4 Key Events

The first case shows simultaneous SUA and STEVE, shows the connection with MPP and suggests IMF guiding of MPP. The second case shows that both UV and visible continua are associated with SUA while Swarm temperature spikes suggest that these continua are thermal emission from optically thin hot plasma.

3.1 March 26, 2008

Figure 2 shows simultaneous visible STEVE emissions seen by the GAKO ASI imager in the NH with SH SUA emissions seen in the vignette of the F16 SSUSI data shown in 2a. The time of the image in 2c is chosen at the F16 SUA crossing time. The image in 2b is chosen at the crossing time of F15. The change in latitude between the two magnetic grids shown in 2b and 2c matches the change in latitude between the F15 and F16 crossings in 2a. In 2l a pair of 6 MeV precipitation spikes (FWHM 19 and 31 km) spaced 160 km apart are crossed by POES-N17 at the same time the image in 2n shows a pair of STEVE streaks. The green grid of magnetic field lines in 2n extends up to the 817 km POES altitude. The magnetic coordinates indicated in red and green in 2n give the best simultaneous fit to the location of STEVE in the MCGR, KIAN

and GAKO ASI images registered and analysed according to (Bennett C. a., 2020). From the angular width and altitude of the overhead STEVE seen in **2n** its “fuzzy” physical width is estimated to be ~ 27 km, reasonably consistent with the 0° precipitation in **2i**. The pair of MeV spikes in **2i** are seen in the overview figure and the MEPED-6 plots from (Bennett C. L., 2021) near 150° W, 60° N as a localized sharp increase in the precipitating flux.

As F15 crossed the SUA its SSJ/4 sensor (only sensitive to precipitating particles) registered a single narrow (19 km) region of precipitating positive ions with an energy flux of just over $2 \text{ erg/cm}^2/\text{s}$ at 7:30:25. No significant precipitation of electrons was seen *in the SSJ data* as the SUA was crossed. A strong upward flow of plasma shown in **2f** was seen with a peak of $2.8 \cdot 10^9 / \text{cm}^2/\text{s}$ at 7:30:10. Near the SUA crossing several significant vectorial changes in the magnetic field are seen, with the differences over the three ranges indicated by dashed lines in figure **2g** drawn in the plane of the SSUSI imagery in figure **2a**. The direction and magnitude of these changes in the magnetic field vector correspond to downward ($\Delta\mathbf{B}1$ and $\Delta\mathbf{B}3$) and upward ($\Delta\mathbf{B}2$) flowing currents at levels shown in the figure. A less complex and even greater downward current is crossed 41 minutes later by the F16 satellite with the magnitude and direction shown in **2a** and **2m**. The widths of all of these FACs are significantly greater than the width of the MeV spikes in **2i**. In all of these current flows, the charge number flux is substantially greater than the 30 eV to 30 keV measured precipitation of either ions or electrons. In both the F15 (shown in **2f**) and F16 (not shown) data, the upward plasma flux level further significantly exceeds the magnitude of the *net* charged particle flux determined from the magnetic field perturbations. The relative westward to upward speed ratio seen in the F15 data in figure **2d** is comparable to the relative westward to upward speed ratio that can be inferred from the ASI data in figure **2c** alone neglecting along (DMSP) track motion. A more quantitative measurement of the absolute upward and westward velocities for the faster drifting STEVE components using triangulation between multiple simultaneous ASI views in the MCGR, KIAN and GAKO sites as a function of time is approximately consistent with the upward and westward velocities shown in figure **2d**.

Since the net charge number flux for the first downward FAC indicated in figure **2g** is three orders of magnitude greater than the precipitating positive particle flux measured in the SSJ/4 sensor, it is concluded that the net current flow must be associated with a large upward flux of negative particles, most likely electrons as predicted by MPP theory. The alternative of a large downward flux of positive particles having energies below the lowest energy channel (30 eV) of the SSJ/4 detector is ruled out, since positive ions with energy below 30 eV would not be able to directly penetrate to the lower altitudes seen at the base of the STEVE luminosity, and are *not* produced in great numbers during the stopping of more energetic particles (in contrast to electrons).

One movie in (Bennett C. L., 2021) shows registered ASI images from the GAKO and MCGR sites. Features such as that labelled “Field Aligned \sim Fixed MLT” in Figure **2c** remain aligned with fixed MLTs near the local average Parker Spiral direction but do not follow transient changes in IMF direction, while other features drift much more rapidly with the visual appearance of “drifting smoke”. Sometimes the “drifting smoke” appears to emerge “out of nothing” from low altitude. In the framework of MPP with energies only above 1 MeV there wouldn’t be visible emissions extending along local magnetic field lines, however, the peak in P_+ seen in **2i** and the particle energy spectrum shown in **2j** suggests that the MPP in this case is accompanied by a population of ~ 30 keV particles. Drifting smoke rising from altitudes below 100 km could be explained by “invisible” MPP producing plasma at low altitude that becomes visible as it rises and recombines while drifting in the local \mathbf{E} cross \mathbf{B} velocity field. Features

remaining at fixed MLT are consistent with the relatively high magnetic rigidity of MeV protons as primaries. A second movie for the 31 Aug 2019 case shows green picket fence features following fixed MLT.

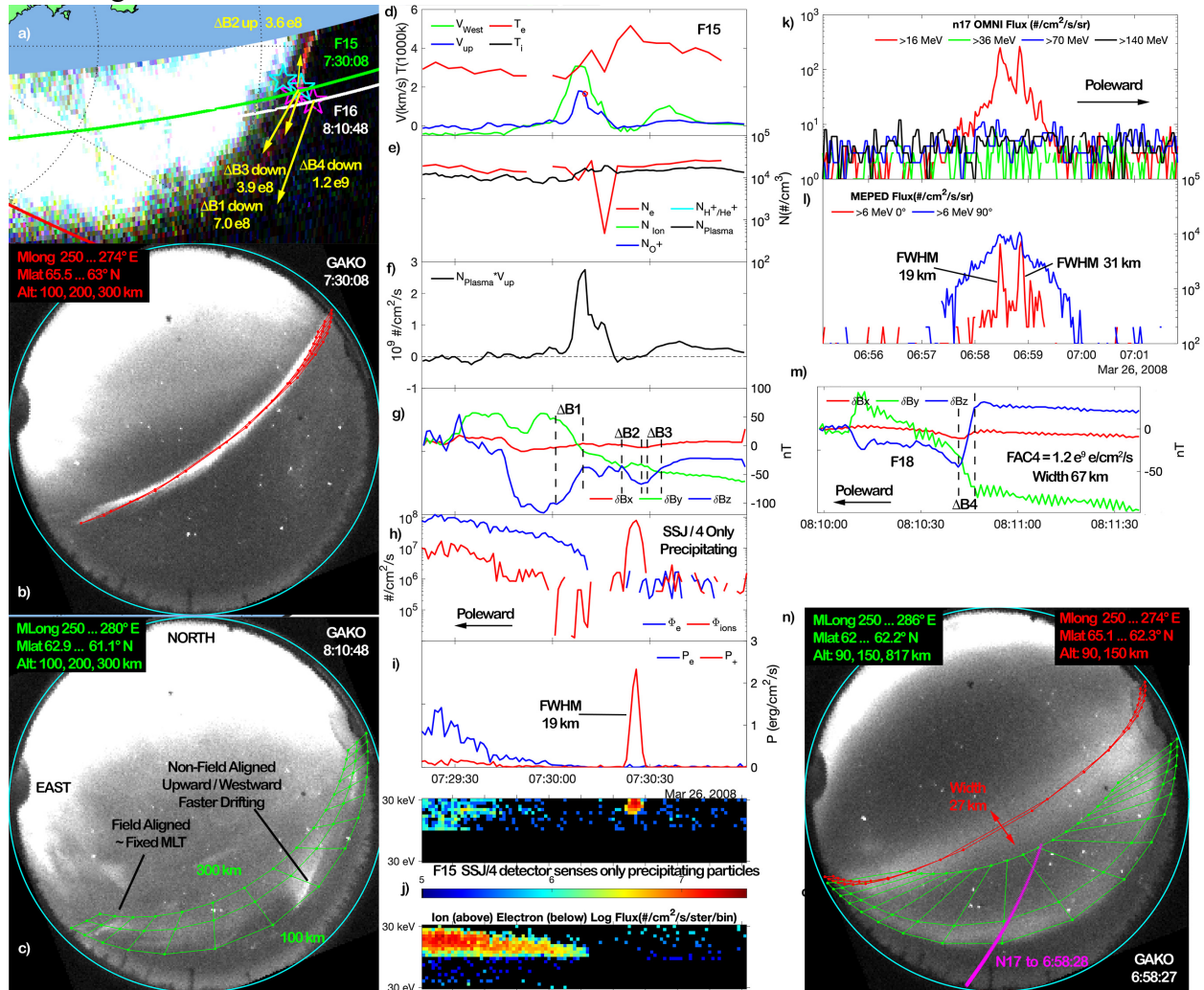


Figure 2. The March 26, 2008 SUA is seen in the SH simultaneously with STEVE in the NH. The SUA is crossed by F15 at 7:30:08 and by F16 at 8:10:48. STEVE is observed from four ASI sites: GAKO, MCGR, KIAN and WHIT so that the three-dimensional structure can be extracted. STEVE was crossed by POES-N17 and two spikes in the 6 MeV proton precipitation channel were observed at 6:58:28 and 6:58:52. At these times, a pair of STEVE streaks are visible in the GAKO, MCGR and WHIT data that are associated with the MeV spikes.

3.2 August 22, 2017

In this event the F16 satellite was operating in full ultraviolet spectral mode so that data with 168 channels covering 1123 Å to 1850 Å of wavelength is available. The spectrum shown in **3o** is derived from the mean value between the times indicated by black lines in **3p** centered at the time 1:31:40 with subtraction of an estimated background derived from an equal time interval split between just before and just after the indicated range indicated by red lines. The spectrum in **3h** is similarly derived from a shorter interval around 3:18:58 shown in **3j**. The negative 1356 Å

peak in **3h** is a background oversubtraction artifact. Because the full UV spectra seen in **3o** and **3h** show no sign of LBH emission bumps, the usual interpretation of the two SSUSI spectral channels covering 1450 ± 50 Å and 1725 ± 75 Å illustrated by the green and blue bars respectively in terms of LBH_{short} and LBH_{long} emissions (Paxton, 2016) is not appropriate for this event. Instead, for this case, and perhaps for many cases in the database for which the SSUSI LBH channels had peaks at SUA crossings, the “LBH” bands provide a measure of the UV continuum emission rather than true LBH band emission. For views off nadir, such as the F16 spectral measurements or the SSUSI DISK measurements away from the ground track, emissions from an altitude greater than the assumed 150 km *appear* at locations further from the nadir ground track. For this reason, the 1356 Å emission seen in **3e**, **3p** and **3j** is determined to be higher than the LBH peaks.

The spike of intensity in the 629.4 nm photometer data as the SUA was crossed is similarly a measure of SUA visible continuum emission. Assuming equal emissivity for visible and UV wavelengths, the visible to UV continua ratio provides an estimate of the temperature of the emitting gas of approximately 8,000 K. This estimate matches the SwA and SwB measured values, but is less than the SwC value.

In this event both Swarm-A (SwA) and Swarm-C (SwC) crossed directly over the SUA, while Swarm-B (SwB) crossed somewhat to the west. The largest SwC temperature spike reaches 2.34 eV with a second 1.32 eV spike crossed 4 seconds later. POES-N15 found an MPP spike shown in **3c** and **3d** as the SUA was crossed. These crossings are particularly remarkable for the narrow width of the spikes in the various readings even without correction for the angle of crossing. The FWHM of the SwA temperature spike was less than 11 km, while the FWHM of the DMSP Nadir Photometer System (NPS) 629.4 nm spike was only 7 km. As the SSUSI scan pixels are 25 km wide, the width of the LBH_L spike in **3e** is clearly less than 25 km and considerably narrower than the 144 km width of the 1356 Å bump. The FWHM of the N15 50 and 100 MeV spikes are 13 & 10 km respectively.

The peak of the >6 MeV 0° data seen in **3d** is over 10^5 protons/cm²/s/sr at 0:35:08. The column ionization rate for this energy flux according to **1e** would be approximately 3×10^{11} /cm²/s. The level of the upward plasma flux shown in **3b** at 1:37:19 is only 1% of this level. This difference is attributed to MPP sporadicity. The SwA and SwC temperature measurements shown in **3k** and **3l** from crossings only 8 seconds apart and from ground tracks only 55 km apart show the temperatures to be sporadic. It is inherent in the MPP theory that sporadic MPP heating be spatially and temporally smeared by multiple scattering and the relative slowness of plasma cooling. These blurring effects can account for the broader distribution of the 630 nm emission seen in **3f** relative to the 629.4 nm emission or the broader 1356 Å emission relative to LBH in **3e**.

SSUSI data is known to be subject to “MeV noise” artifacts, in which penetrating ionizing radiation produces signals that are not true UV light. This artifact is best recognized by its spread across all columns of the DISK and LIMB data. The fact that the 427 nm and 629 nm bumps in the NPS instrument (not subject to “MeV noise”) between 1:37 and 1:38 shown in **3f** and the P- and P+ bumps from the SSI instrument (also not subject to “MeV noise”) shown in **3g** coincide in shape with the MeV noise in the SSUSI data indicates that the SSUSI instrument is partially functioning as a crude, uncalibrated, omni-directional MeV detector. For this reason, MPP can be inferred from DMSP data alone, even without simultaneous and collocated POES observations.

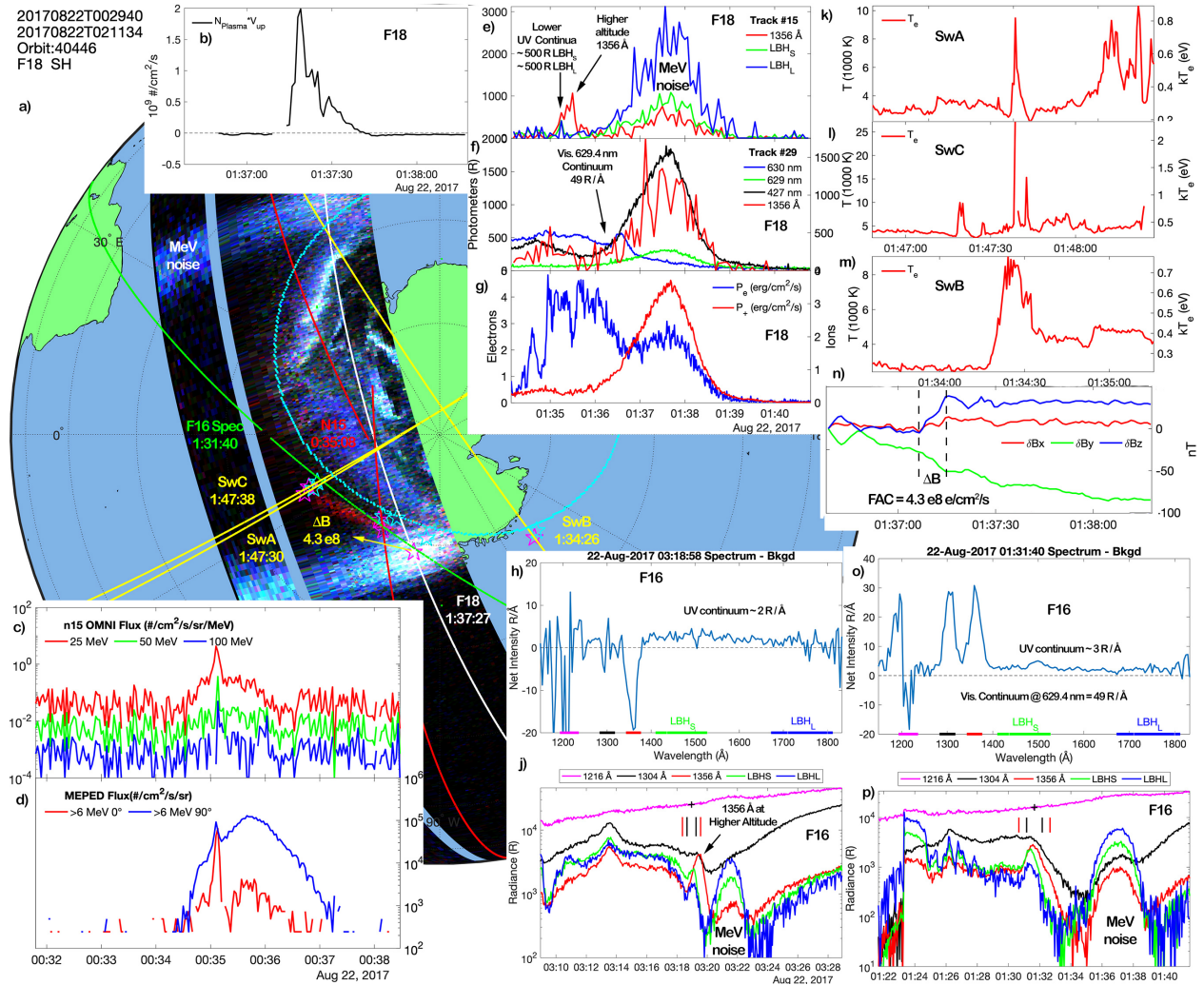


Figure 3. The August 22, 2017 event observed by six satellites is illustrated here and discussed in the text.

5 Conclusion

Solar MeV protons with comoving keV electrons following Parker spirals impinging on the earth's atmosphere can explain the MLT location, hemispheric asymmetry, continuum UV and visible emissions, upwelling plasma flux, downward FACs and ephemeral picket fence features of STEVE. It was observed that IMF guided MPP, as evidenced by POES MeV precipitation and Swarm Temperature spikes, was not restricted to subauroral regions. Assuming the theory is correct, many more cases similar to those exhibited in the (Bennett C. L., 2021) database remain to be found. Study of such cases could greatly expand the understanding of solar MeV emissions.

Acknowledgments, Samples, and Data

- The author declares no competing interests.

- DMSP SSJ, SSM and SSIES data are available from <https://satdat.ngdc.noaa.gov/dmsp/>
- DMSP SSUSI data are available from <https://ssusi.jhuapl.edu/>
- ASI data are available from <https://data-portal.phys.ucalgary.ca/>
- POES data are available from <https://ngdc.noaa.gov/stp/satellite/poes/>
- GOES data are available from <https://ngdc.noaa.gov/stp/satellite/goes/>
- IMF data are available from <http://omniweb.gsfc.nasa.gov>
- Swarm data can be obtained at <http://earth.esa.int>

References

Bibliography

- Archer, W. G.-L.-M. (2019). Steve: The Optical Signature of Intense Subauroral Ion Drifts. *Geophysical Research Letters*, 46, 6279-6286. doi: 10.1029/2019GL082687.
- Archer, W. S.-L. (2019). The Vertical Distribution of the Optical Emissions of a Steve and Picket Fence Event. *Geophysical Research Letters*, doi:10.1029/2019GL084473.
- Bennett, C. a. (2020). Improved Analysis of STEVE Photographs. *Journal of Geophysical Research*, doi:10.1029/2020JA027843.
- Bennett, C. L. (2021). *Collection of Ultraviolet STEVE observations*. Retrieved from <https://doi.org/10.6084/m9.figshare.c.4824723.v1>
- Berger, M. C. (2017, July doi:10.18434/T4NC7P). Stopping-Power & Range Tables for Electrons, Protons, and Helium Ions. Retrieved from <https://www.nist.gov/pml/stopping-power-range-tables-electrons-protons-and-helium-ions>
- Bethe, H. (1930). Zur Theorie des Durchgangs schneller Korpuskularstrahlen durch Materie. *Annalen der Physik*, doi:10.1002/andp.19303970303.
- Chu, X. D.-L. (2019). Identifying the magnetospheric driver of STEVE. *Geophysical Research Letters*, doi:10.1029/2019GL082789.
- Ding, G.-X. H.-X. (2016). A new auroral boundary determination algorithm based on observations from TIMED/GUVI and DMSP/SSUSI. *JGR: Space Physics*, doi:10.1002/2016JA023295.
- Edgar, B. M. (1973). Energy Deposition of Protons in Molecular Nitrogen and Applications to Proton Auroral Phenomena. *Journal of Geophysical Research*, doi:10.1029/JA078i028p06595.
- Gallardo-Lacourt, B. L. (2018). On the Origin of STEVE: Particle Precipitation or Ionospheric Skyglow? *Geophysical Research Letters*, 1-6, doi.org/10.1029/2018GL078509.
- Gallardo-Lacourt, B. N. (2018). A Statistical Analysis of STEVE. *Journal of Geophysical Research: Space Physics*, 9893-9905, doi: 10.1029/2018JA025368.
- Gillies, D. D.-L. (2019). First Observations From the TReX Spectrograph: The Optical Spectrum of STEVE and the Picket Fence Phenomena. *Geophysical Research Letters*, 7207-7213, doi: 10.1029/2019GL083272.
- Gillies, D. L. (2020). The Apparent Motion of STEVE and the Picket Fence Phenomena. *Geophysical Research Letters*, 47, doi: 10.1029/2020GL088980.
- Itikawa, Y. (2006). Cross Sections for Electron Collisions with Nitrogen Molecules. *Journal of Physical and Chemical Reference Data*, 35, doi: 10.1063/1.1937426.
- Itikawa, Y. (2009). Cross Sections for Electron Collisions with Oxygen Molecules. *Journal of Physical and Chemical Reference Data*, 38, doi: 10.1063/1.3025886.
- Jursa, A. S. (1985). *Handbook of Geophysics and the Space Environment*. Air Force Geophysics Laboratory.
- Liang, J. D.-M.-L. (2019). Optical Spectra and Emission Altitudes of Double-Layer STEVE: A Case Study. *Geophysical Research Letters*, doi:10.1029/2019GL085639.
- MacDonald, E. E.-L. (2018). New science in plain sight: Citizen scientists lead to the discovery of optical structure in the upper atmosphere. *Science Advances*, 1-5, doi: 10.1029/2019GL086145.
- Mende, S. a. (2019). Color Ratios of Subauroral (STEVE) Arcs. *Journal of Geophysical Research: Space Physics*, doi:10.1029/2019JA026851.

- Mende, S. H. (2019). Subauroral Green STEVE Arcs: Evidence for Low-Energy Excitation. *Geophysical Research Letters*, doi:10.1029/2019GLO86145.
- Nishimura, Y. G.-L. (2019). Magnetospheric Signatures of STEVE: Implications for the Magnetospheric Energy Source and Interhemispheric Conjugacy. *Geophysical Research Letters*, 5637-5644, doi: 10.1029/2019GL082460.
- Nishimura, Y. Y. (2020). Magnetospheric Conditions for STEVE and SAID: Particle Injection, Substorm Surge, and Field-Aligned Currents. *JGR Space Physics*, doi:10.1029/2020JA027782.
- Parker, E. (1963). *Interplanetary Dyamical Process*. New York: Interscience.
- Paxton, L. S. (2016). Far ultraviolet instrument technology. *JGR: Space Physics*, doi:10.1002/2016JA023578.
- Solomon, S. (2017). Global modeling of thermospheric airglow in the far ultraviolet. *JGR Space Physics*, doi: 10.1002/2017JA024314.